Low-Field X-Band EPR Transitions of LiF : Mn^{2+}

C. Gago-Bousquet, M. Garcia-Sucre, and A. Serra-Valls
Instituto Venezolano de Investigaciones Científicas,
Departamento de Física Atómica y Molecular, Apartado 1827, *Caracas, Venezuela*
(Received 13 March 1972)

Low-field transitions of LiF : Mn^{2+} are studied in the X band. These transitions, for the relatively simple situation when the magnetic field is parallel to a cubic axis, are analyzed and attributed to two paramagnetic centers already known from previous works in X and J bands. One of these centers has an orthorhombic symmetry and yields forbidden transitions of the type $\Delta\langle S_z\rangle = \pm 2, \pm 3, \ldots$, superimposed on some of the allowed transitions of a low-concentration center of tetragonal symmetry. The forbidden transitions produce the largest contribution to the spectrum. Because of the importance of the crystal field terms involved, the exact diagonalization of a Hamiltonian including Zeeman, crystal field, and hyperfine terms, provides the zero-order eigenfunctions for the perturbation treatment of the resolved superhyperfine interactions with the F^- ligands. The validity of the first-order approximation is established by explicit consideration of the second-order terms which in most cases are found to be negligible. A general good agreement is found between the experimental and calculated spectra. Further study of forbidden transitions in this and similar systems, leading to information not accessible in the allowed spectra, appears feasible.

I. INTRODUCTION

Electron paramagnetic resonance (EPR) forbidden transitions have been observed rarely in alkali halides. Most of the work done has been concerned with hyperfine (hf) transitions of the type $\Delta M = \pm 1$ and $\Delta m \neq 0$ (see, e.g., Ref. 1) occurring in the midst of the allowed ones. In the case of paramagnetic centers displaying superhyperfine (shf) interactions the study of forbidden transitions has not been undertaken so far. Here observations are possibly only on those lines lying outside the region of the allowed spectrum, i.e., $\Delta M = \pm 2, \pm 3, \ldots$. There are several of such systems in which the crystal fields (cf) involved would induce this type of forbidden transitions with enough intensity to be observable in X band by means of the electronic averaging of successive sweeps.

Several treatments of forbidden transitions are available in which the cf and/or the hf terms are considered as perturbations (see, e.g., Refs. 2–4). Although they could yield a good approximation in part of the present work, in general the requirements of perturbation theory are not fulfilled and the position and intensities of the lines will be obtained from the exact diagonalization of a Hamiltonian $\mathcal{H}_0$ including Zeeman, cf, and hf terms.

On the other hand shf interactions terms yield a resolved structure and, as it will become clear later, they may be treated as a first-order perturbation to $\mathcal{H}_0$. Some consideration should be given to their second-order effects because they may be observable under certain experimental conditions; also, they are required in order to establish accurately the validity of the first-order approximation. Furthermore, since the Zeeman term is not predominant, especially at the lower fields, a certain dependence of the shf splittings on the magnetic field is to be expected.

Previous work at 9.5[5] and 35 GHz[6] has determined the symmetry and Hamiltonian parameters of an orthorhombic center in LiF : Mn^{2+}, involving a chemical impurity X^- nearest to the Mn^{2+} and a Li^+ vacancy in second-neighbor position[7] [Fig. 1(a)]. A second center of tetragonal symmetry in very low concentration has also been observed [Fig. 1(b)] and its parameters have been measured.[6] Using this information, the low-field transitions at 9.5 GHz were interpreted as forbidden transitions of the orthorhombic center superimposed on the allowed transition of the low-concentration tetragonal center.

In what follows, our treatment of the forbidden transitions will be specialized to the case of the above orthorhombic center in LiF : Mn^{2+}, when the magnetic field is parallel to the cubic axes. The features and difficulties encountered may be considered, however, typical of those to be expected in other cases.

II. EXPERIMENTAL

A conventional reflection X-band spectrometer using a rectangular cavity operating at 9.4882 GHz in the Te_{102} mode and with 100-KHz field modulation was used. The signal-to-noise ratio was enhanced by accumulating sweeps in an electronic averaging device (Computer of Average Transients or CAT), triggered at the beginning of each sweep by the signal from a proton probe. Linear sweeps of 100 G/min were used. An external pulse gener-

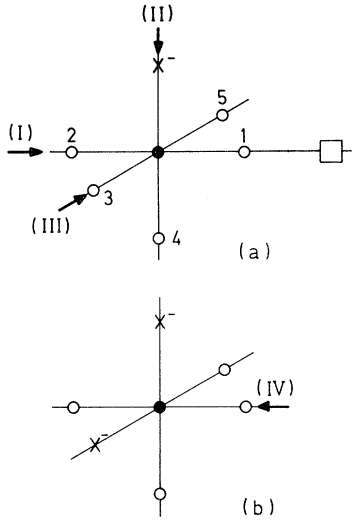

FIG. 1. Models for the two kinds of centers involved. Heavy arrows (I to IV) show the directions of the magnetic field corresponding to the spectra in Fig. 3. Closed and open circles stand for Mn^{2+} and F^- atoms, respectively, and the open square in (a) represents a Li^+ vacancy. Forbidden transitions belong to the orthorhombic center (a) where 1 to 5 refer to the numbering of F^-'s used in Sec. III. The tetragonal center (b) yields the allowed spectrum of weak intensity.

ator was used to advance the CAT addresses. The sample was a $3\times3\times9$-mm LiF single crystal doped in the melt with 10^{-3} Mn^{2+} added as $MnCl_2$.[8] A magnetic field interval from 130 to 1360 G was explored at room temperature and the crystal oriented with its [100] axis parallel to the magnetic field. This orientation was chosen because the crystal field term attains its maximum value as was established from observations on the allowed spectra,[5,6] the six possible kind of spectra are reduced to three equally abundant ones, spectral sensitivity to misalignment errors is minimum, and the shf patterns involved are simpler.

III. THEORETICAL

The total Hamiltonian describing the system can be written

$$\mathcal{H}=\mathcal{H}_0+\sum_n \mathcal{H}_F^{(n)} , \tag{1}$$

where the summation term represents the resolved interaction with the ligands around the Mn^{2+}. For $\vec{H}$ parallel to the cubic axes and ignoring a constant term, the predominant part $\mathcal{H}_0$ can be written

$$\mathcal{H}_0=g\mu_B HS_z+g_0 S_z^2+g_2(S_+^2+S_-^2) +A I_z S_z+\tfrac{1}{2}A(S_+ I_-+S_- I_+) , \tag{2}$$

where g_0 and g_2 are given in Table I for the three different and equally abundant orientations of the paramagnetic center. The numerical values of the cf and hf parameters involved in Eq. (2) are given by[6] $D=436\pm6$ G, $|E|=110\pm2$ G, and $A=-92.5\pm0.5$ G, with $g=2.030\pm0.001$. Small terms such as the quadrupolar, nuclear Zeeman, quartic cf, and those coming from the anisotropy of the hf tensor, will be neglected. A computer program diagonalizes $\mathcal{H}_0$ in a standard $|M\rangle|m\rangle$ basis set and obtains its eigenvalues E_N and eigenfunctions $|N\rangle$ together with the position H_0 of each EPR transition, its relative probability $P(H_0)$ and certain matrix elements required in the calculations.[9] From properties of terms in Eq. (2) it can be easily shown that eigenfunctions $|N\rangle$ split in two different kinds $|N;+1\rangle$ or $|N;-1\rangle$ in which all the $|Mm\rangle$'s involved are such that $M+m$ is always odd or even, respectively. From this the following two relations are obtained:

$$\langle N';k'|S_z|N;k\rangle\propto\delta_{k',k} \tag{3}$$

and

$$\langle N';k'|S_\pm|N;k\rangle\propto\delta_{k',-k} , \tag{4}$$

where $k, k'=\pm1$ are eigenvalues of the time-reversal operator. These relations will be used in the perturbation treatment of the shf structure.

The nth term in the shf Hamiltonian appearing in Eq. (1) is given by[10]

$$\mathcal{H}_F^{(n)}=\vec{I}^{(n)}\cdot\underline{A}'^{(n)}\cdot\vec{S}+g_n\mu_N\vec{H}\cdot\vec{I}^{(n)} , \tag{5}$$

where $I^{(n)}=\frac{1}{2}$, (n) refers to the nth fluorine and runs from 1 to 5 [Fig. 1(a)]. The components of $\underline{A}'^{(n)}$ along the σ and π axes will be noted A' and B', respectively. Following the assumptions of Ref. 6, the principal axes of the tensors $\underline{A}'^{(n)}$ will be assumed to be parallel to the cubic axes. Furthermore, except for fluorine 4, the A' and B' values will be taken to be the same for all fluorine.[11]

An extended basis $|N\rangle|\nu\rangle$ will be used to handle the additional quantum numbers associated with the nuclear magnetic moment of the ligands, where, in general, the $|\nu\rangle$'s are appropriate linear com-

TABLE I. Crystal field parameters for three different orientations I, II, and III of the orthorhombic center; p and q refer to the axes perpendicular to the D axis; these three axes have been taken parallel to the cubic ones. The numerical values of the parameters involved are $D=436\pm6$ G, $|E|=110\pm2$ G ($g_e/g=0.9864\pm0.0005$).

	g_0	g_2
$\vec{H}\parallel\vec{D}$ axis (I)	D	$-\frac{1}{2}\|E\|$
$\vec{H}\parallel\vec{p}$ axis (II)	$-\frac{1}{2}(D+3\|E\|)$	$\frac{1}{4}(D-\|E\|)$
$\vec{H}\parallel\vec{q}$ axis (III)	$-\frac{1}{4}(D-3\|E\|)$	$\frac{1}{4}(D+\|E\|)$

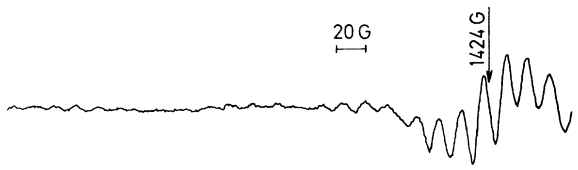

FIG. 2. Low-field region at 9.5 GHz, no CAT used, showing the beginning of the allowed spectrum at right and some of the weak intensity lines, $s/n \sim 2$, discussed in the text.

binations of $\prod_n |m_n\rangle$ functions; $|m_n\rangle$ being the eigenfunctions of $I_z^{(n)}$. In a first-order approximation and using relation (4) the diagonal elements of the perturbing term given by Eq. (5) yield

$$\langle Nm_n | \mathcal{H}_F^{(n)} | Nm_n\rangle = m_n [a_n' \tilde{M}(N) + g_n \mu_N H] , \quad (6)$$

where a_n' equals A_n' or B_n' if the (n) axis, respectively, is parallel or perpendicular to $\vec{H}$, and $\tilde{M}(N) \equiv \langle N | S_z | N\rangle$. Because of the extensive admixing of functions $|M\rangle |m\rangle$, $\tilde{M}$ is no longer a good quantum number; but in order to keep a parallelism with the usual treatment we shall use $\Delta\tilde{M}$ to characterize transitions. Selection rule $\Delta m_n = 0$, for all n, strictly holds for the shf structure. Up to first order, the shf displacements in a $|N'\nu\rangle \rightarrow |N\nu\rangle$ transition, are

$$\delta H_1 = -f_1 \sum_n a_n' m_n , \quad (7)$$

with

$$\frac{1}{f_1} \equiv \frac{\Delta dE_N/dH_0}{\Delta\tilde{M}_0} + \frac{d}{dH_0}(\ln\Delta\tilde{M}_0)\sum_n a_n' m_n , \quad (8)$$

where Δ takes the difference between quantities associated, respectively, with states $|N'\rangle$ and $|N\rangle$ and evaluated at $H = H_0$. Usually, for allowed transitions the factor f_1 is very close to unity. On the other hand, for forbidden transitions it may change somewhat from one transition to another (see Sec. IV). These variations of f_1 come from nonlinearities of the energy levels with the magnetic field (Fig. 4) and the fact that $\tilde{M}$ is no longer a good quantum number.

The calculation of second-order effects can be carried out using standard methods of degenerate perturbation theory (see, e.g., Ref. 12). However, since these effects turned out to be negligible for levels involved in all the relevant transitions, only some details are given in the Appendix

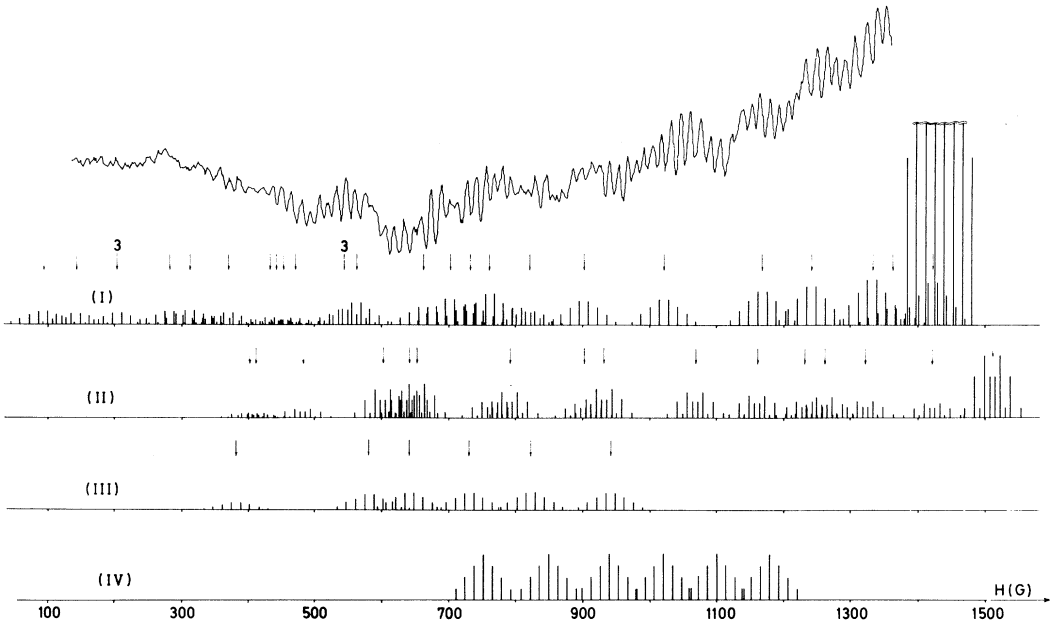

FIG. 3. The experimental (CAT output) and calculated spectra (I), (II), and (III) are the forbidden spectra corresponding, respectively, to the orientations illustrated in Fig. 1. In (I) the first allowed transition is shown for reference at right-hand side and the shf packets centered beyond 1500 G are omitted. A few lines with relative intensity less than 0.008 times the intensity of the allowed packet are omitted for fields higher than 600 G. The shf splittings are represented taking factor f_1 in Eq. (7) equal to unity. In the scale used, this may be innacurate only for the low-field packets. Vertical arrows indicate the centers of the shf packets. The number 3 appearing over two arrows in (I) indicates the near coincidence of three transitions. The allowed weak-intensity spectrum (IV) is drawn with a somewhat exaggerated intensity. For I and III the shf structure used are $1:3:5:7:7:\cdots$ split by 13.7 G; $1:0:4:1:6:4:4:\cdots$ split by 16 G for II; and $1:2:3:4:3:\cdots$ split by 14 G for IV. The slow rise in the zero line of the experimental spectrum is due to the proximity of the first allowed lines. $\hbar\omega_k/g\mu_B = 3339 \pm 2$ G.

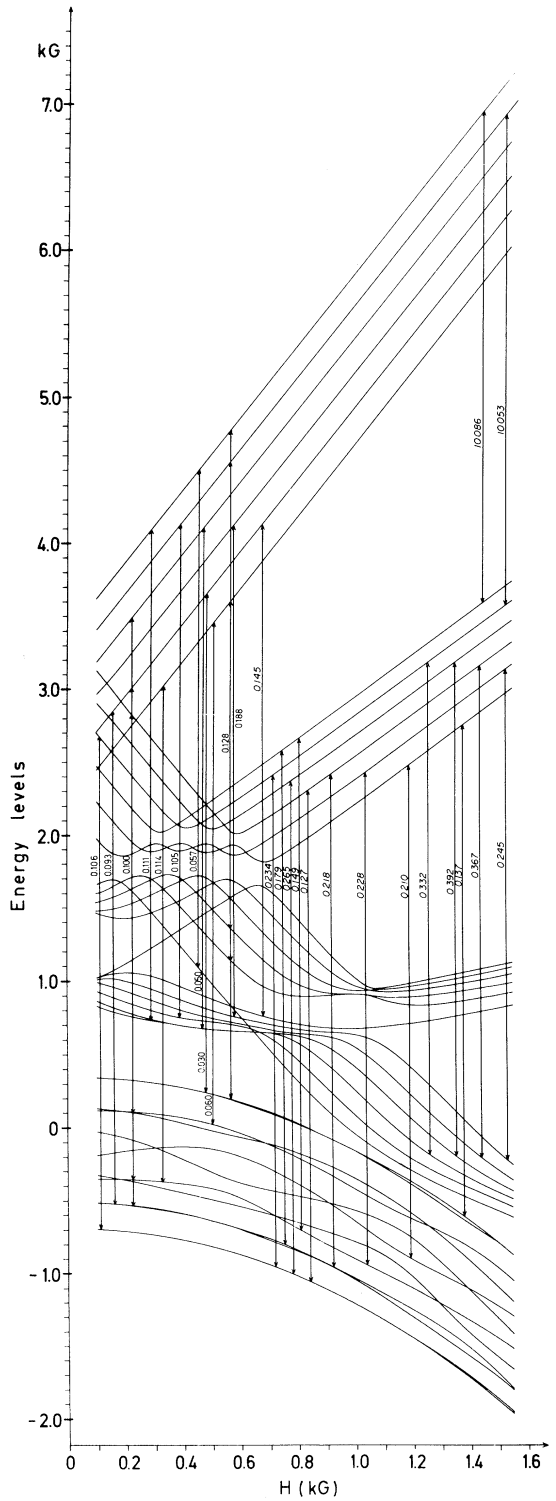

FIG. 4. Energy-configuration diagram for spectrum I (H parallel to D axis) indicating the position of the center of the different shf packets and their relative intensities. The two first allowed transitions are shown at right. A few forbidden transitions with intensities less than 0.008 relative to the allowed ones are omitted beyond 600 G.

for the case of orientation I [Fig. 1(a)]. As a rough rule it was found that second-order effects can be important only when[13]

$$\left| A' \sum_{N' \neq N} \frac{\langle N | S_q | N' \rangle \langle N' | S_{q'} | N \rangle}{E_N - E_{N'}} \right| \gtrsim 1 , \qquad (9)$$

where $q, q' = z, -, +$.

IV. RESULTS

The experimental spectra show weak transitions from 130 to 1360 G. Some of these transitions were visible even without the use of the CAT [Fig. (2)] with signal-to-noise ratio between 1 and 2. The intensity of the spectra within the region studied was enhanced by a factor of $(250)^{1/2}$. Moreover, because of technical problems related with the triggering signal, the enhancement obtained by the CAT between 130 and 400 G was about one-half that for the rest of the spectra.

Exploration with the CAT in the high-field side beyond 5400 G shows the presence of a hf sextet much weaker in intensity than the transitions at low fields, which suggests the existence of a second allowed spectrum arising from a low-concentration center. This point was checked by experiments[6] at 35 GHz which confirm the presence of a tetragonal center with $D = 604 \pm 7$ G and concentration about $\frac{1}{10}$ the concentration of the orthorhombic center. Exploration at this frequency of high- and low-field regions did not indicate the existence of other centers. Therefore, we can expect to find that at 9.5 GHz this center yields weak-intensity allowed transitions within the region of consideration (from 760 to 1180 G).

The experimental spectrum of Fig. 3 is very complex and has a high number of transitions distributed in the magnetic field in a way which greatly differs from the regularities encountered in allowed spectra. The splittings among the experimental shf lines range from 11 to 18 G (~14 G being a typical value), and the Γ_{pp} from 5 to 10.5 G (~8.5 being a typical value). Furthermore, the abrupt intensity variation of neighboring lines in certain regions of the spectrum, suggests the overlap of shf packets. The linewidths of forbidden transitions may be expected to be essentially similar to that of the allowed ones, since the main contribution to the linewidth can be attributed to unresolved interactions with the neighbors. This includes the interaction with impurity X^-, which is very likely to be OH^-.[14]

The model proposed in Sec. III, and the parameters therein, yield three kinds of forbidden spectra corresponding to different orientations of the orthorhombic center. For the forbidden lines the calculated intensity ranges from about 0.01 to 0.04 times the intensity of the outermost allowed tran-

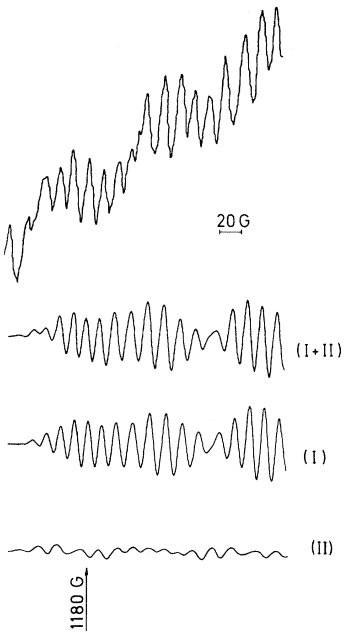

FIG. 5. Calculated and experimental envelopes in the range 1120–1360 G. Here forbidden transitions arise from spectra I and II only. To obtain spectra I Gaussian line-shape derivatives with $\Gamma_{pp}=7.4$ G were used for the lines of shf packets centered at $H_0=1174$, 1245, 1337, and 1366 G. A first-order approximation was used to obtain the shf splittings; small variations (~10%) due to the nonlinearity of energy levels with H, were considered. Similarly, spectra II were reconstructed centering shf packets at $H_0=1165$, 1233, 1265, 1323 G and using Gaussian derivatives with $\Gamma_{pp}=10$ G; no variation in the splittings was found. The center of the first shf packet of the allowed weak spectrum IV (not taken into account) is shown at $H_0=1180$ G.

sitions of the orthorhombic center. These lines should be easily observable after $N=250$ sweeps according to the following formula, which compares the signal-to-noise ratio (s/n) for a forbidden (F) and an allowed (A) transition:

$$\left(\frac{s}{n}\right)_F \sim \left(\frac{s}{n}\right)_A \frac{i_A}{i_F} \frac{(\Gamma_{pp})_A^2}{(\Gamma_{pp})_F^2} \sqrt{N} \ . \qquad (10)$$

In this expression, $i_{A,F}$ are the calculated intensities. Thus, in our case we have

$$0.1/10 \lesssim i_F/i_A \lesssim 0.4/10 \ .$$

Besides, for the central shf lines of the type-I allowed packet experimentally one has $(s/n)_A \sim 20$, which yields $3 \lesssim (s/n)_F \lesssim 13$. Therefore, the calculated forbidden lines should be visible after 250 sweeps with the signal-to-noise ratio found experimentally, provided that they are not excessively widened (Fig. 5).

The orientation with the magnetic field parallel to the vacancy axis (structure I) is by far the one which contributes the most to the forbidden spectra (Fig. 5). The energy correlation diagram for this orientation, without including the shf structure, is given in Fig. 4. From this diagram and using Eq. (7), we have calculated the shf splittings for the structure I. Similar calculations were carried out for II and III.

The calculation shows for the relevant transitions that the left-hand member of relation (9) is less than 3×10^{-2}. Therefore, second-order effects can be neglected, i.e., shf interactions can be accounted to a very good accuracy by the first-order approximation.

Figure 3, where the first-order approximation with $f_1=1$ is used, shows a general good agreement between experimental and calculated spectra. A reconstruction of the experimental envelope was

TABLE II. Partial list of forbidden transitions corresponding to a Hamiltonian $\mathcal{H}_0$ which includes Zeeman, crystal-field, and hyperfine terms. The transitions shown arise from three possible orientations I, II, and III of an orthorhombic center. H_0 and P are the position and relative intensity of transitions, respectively. $\tilde{M}$, $\tilde{M}'$ and $\tilde{m}$, $\tilde{m}'$ are diagonal elements of S_z and I_z, respectively, involving the eigenfunctions corresponding, in each case, to the two levels linked by a transition. Errors in H_0 arise from uncertainties in the Hamiltonian parameters and from the ±5-G accuracy of the calculation. In I the forbidden transitions belonging to the range 200–1370 G and with relative intensity $P \geq 0.15$, or else intensities arising from near coincidence of several transitions are shown. Several ones involving a quasidegenerate level are also included for illustrative purposes and an index d indicates this type of transitions. In II and III all transitions in the range 120–1400 G, respectively, with $P > 0.14$ and $P > 0.13$ are included.

	H_0 (G)	$\tilde{M}'$	$\tilde{M}$	$\tilde{m}'$	$\tilde{m}$	P
I						
d	201 ± 16	−0.225	−2.368	−0.075	2.467	
	205 ± 13	2.375	−0.419	1.527	−1.017	0.100[a]
d	201 ± 17	2.443	0.306	−0.477	−0.374	
d	286 ± 13	2.470	−0.484	−2.490	−1.230	0.111
	441 ± 6	2.475	−2.346	−2.491	−2.495	0.057
d	551 ± 6	2.469	−1.962	−1.486	−1.643	
d	551 ± 6	2.477	−2.097	−2.492	−0.609	0.128[a]
d	547 ± 13	2.475	−0.583	2.500	0.712	
	567 ± 13	2.463	−0.497	0.515	1.009	0.188
	667 ± 13	2.470	−0.534	1.509	2.235	0.145
d	701 ± 7	1.380	−0.758	−1.454	−0.792	0.234
	741 ± 7	2.469	−1.862	0.513	0.290	0.053
	731 ± 7	1.417	−0.787	−2.472	0.366	0.179
d	761 ± 6	1.368	−0.822	−0.452	−0.840	0.265
	794 ± 6	1.424	−1.100	−2.475	−0.965	0.149
d	902 ± 6	1.392	−0.945	0.533	−0.517	0.218
	1023 ± 6	1.416	−1.002	1.515	0.203	0.228
	1176 ± 5	1.431	−1.402	0.522	0.127	0.081
	1174 ± 6[b]	1.448	−1.065	2.493	1.117	0.210
	1245 ± 5[b]	1.446	−1.380	−1.478	−0.386	0.332
	1337 ± 5[b]	1.445	−1.480	−0.478	0.417	0.392
	1366 ± 5[b]	1.462	−1.411	2.494	1.267	0.137
	1410 ± 25[c]	2.488	1.463	−2.495	−2.487	10.085

TABLE II. (*Continued*).

H_0(G)	$\tilde{M}'$	$\tilde{M}$	$\tilde{m}'$	$\tilde{m}$	P
II					
600 ± 7	0.680	−1.274	0.672	1.504	0.239
639 ± 6	0.720	−1.219	−0.742	−0.529	0.230
651 ± 7	0.754	−1.362	−0.667	−2.485	0.292
933 ± 5	1.078	−1.283	0.412	1.455	0.247
1074 ± 5	1.248	−1.315	0.752	2.466	0.223
1165 ± 5[b]	1.345	−1.341	0.643	2.470	0.197
1233 ± 6[b]	1.067	−1.401	−1.464	−0.516	0.136
1265 ± 5[b]	1.430	−1.364	1.398	2.474	0.177
1323 ± 6[b]	1.031	−1.396	−0.484	0.479	0.144
III					
584 ± 8	0.589	−2.053	−2.446	−2.410	0.1302
643 ± 8	0.572	−1.900	−1.446	−1.490	0.137
733 ± 8	0.557	−1.878	−0.465	−0.591	0.138
823 ± 8	0.559	−1.880	0.511	0.349	0.144
944 ± 8	0.567	−1.943	1.485	1.342	0.141

[a]Resultant intensity of three nearly coincident transitions.

[b]These transitions were considered in the reconstruction of the envelope shown in Fig. 7.

[c]First allowed transition.

done in the region between 1120 and 1360 G in which there is superposition between transitions belonging to the spectra I and II (Fig. 5). The shf splittings were obtained from Eq. (7). For the spectrum of structure I, the factor f_1 predicts small variations in the splittings, within ± 10%, while for spectrum II this factor is very close to unity. The second term in f_1 turns out to be negligible in both cases. The second-order contribution to the shf displacements [see Eq. (A8) of Appendix] may affect somewhat the outer lines in each shf packet in spectrum I while leaving the central lines almost unaffected. We have thus neglected this correction. The reconstructed envelopes of Fig. 5 clearly show that in the superposition of the spectra I and II, to obtain the experimental envelope, the spectrum I predominates.

Table II gives the calculated central positions H_0, $\tilde{M}'$, $\tilde{M}$, and relative intensities of several important transitions. Since most of the relevant ones are of the type $\tilde{M} \rightleftharpoons \tilde{M}' \sim -\tilde{M}$ their calculated H_0 values remain almost unaffected by the uncertainty in the parameters D and E. However, in some others (mostly of weak intensity, and at low field) this yields the largest contribution to the over-all error in H_0.

In general the program yields H_0 within ± 5-G accuracy, a precision comparable to that of experiment. The influence of the small terms neglected in Eq. (2) was found to be entirely within this range of uncertainty.

The superposition of the allowed (IV) on the already complex forbidden spectra greatly hinders the attainment of additional information about the parameters involved.[15] However, this information may be available under different experimental conditions.

V. CONCLUSIONS

A good agreement was found between the low-field experimental spectra and the calculated ones. The latter comprise the forbidden transitions of an orthorhombic center superimposed on the allowed lines of a low-concentration tetragonal center.

For the considered magnetic field orientation, the shf interaction can be treated to a very good approximation as a first-order perturbation, ever since the second-order effects are in general exceedingly small. Even in a first-order approximation the shf splittings can be expected to change somewhat from one packet to another.

It becomes apparent from this work that the study of EPR forbidden transitions in LiF is feasible and that it could yield additional information not available by merely focusing our attention on the allowed spectra.

ACKNOWLEDGMENTS

Many thanks are due to Dr. G. Blanc for experimental assistance in the initial stages of this work, to Dr. G. Oliver for providing us with a diagonalizing subroutine, and to G. Mata, J. Serra, and F. Kaiser for technical help. Special recognition goes to the Universidad Central de Venezuela Computational Center.

APPENDIX: SECOND-ORDER EFFECTS

Second-order effects, both on the energy levels and on the selection rules, are determined by the

TABLE III. Matrix elements $\langle\lambda'|F_{\pm}^2|\lambda\rangle$ involved in the calculation of the superhyperfine second-order effects. The operator involved in the mixing of states $|\lambda\rangle = |I^a; m_a\rangle |I^b; m_b\rangle |m_4\rangle$ is $F_{\pm} = \frac{1}{2}B' I_{\pm}^a + \frac{1}{4}(A'+B')(I_{\pm}^b + I_{\pm}^{(4)}) + \frac{1}{4}(A'-B') \times (I_{\mp}^b - I_{\mp}^{(4)})$, where $I^a = I^{(1)} + I^{(2)}$, $I^b = I^{(3)} + I^{(5)}$, and $I^{(n)}$ has been associated with the Mn^{2+} $-n$th ligand (1 and 2 ligands are on the axis parallel to the magnetic field). $\Delta m_l \equiv m_l' - m_l$, where $l = a, b, 4$. Condition $(I^l)' = I^l$ is implicit. Matrix elements for cases $\Delta m_a = \Delta m_4 = 0$, $\Delta m_b = \pm 2$; $\Delta m_a = 0$, $\Delta m_b = \Delta m_4 = \pm 1$; and $\Delta m_a = -\Delta m_b = \mp 1$, $\Delta m_4 = 0$, are obtained, respectively, from the formula appearing in second to fifth row, by changing the sign of m_b, m_4, $\sqrt{2}$, and B'.

Δm_a	Δm_b	Δm_4	$\langle\lambda'\|F_{\pm}^2\|\lambda\rangle$	
±2	0	0	$\sqrt{2}\,\delta_{m_{a'},\mp 1}(\frac{1}{2}B')^2$	
0	±2	0	$2\delta_{mb,\mp 1}$	$\times[\frac{1}{4}(A'+B')]^2$
0	±1	±1	$2\sqrt{2}(\delta_{m_{b,0}} + \delta_{m_{b,\mp 1}})\delta_{m_{4,\mp 1/2}}$	
±1	±1	0	$2(\delta_{m_{b,0}} + \delta_{m_{b,\mp 1}})$	$\times(\delta_{m_{a,0}} + \delta_{m_{a,\mp 1}})\, B'\frac{1}{4}(A'+B')$
±1	0	±1	$\sqrt{2}\,\delta_{m_{4,\mp 1/2}}$	

TABLE IV. Matrix elements $\langle\lambda'|F_{\pm}F_{\mp}|\lambda\rangle$ involved in the calculation of the shf second-order effects. Cases $\Delta m_a=\Delta m_b=\pm 1$, $\Delta m_4=0$, and $\Delta m_a=\Delta m_4=\pm 1$, $\Delta m_b=0$ are obtained, respectively, from the first and second rows by reversing the sign of m_b, m_4, $\sqrt{2}$, and B'.

Δm_a	Δm_b	Δm_4	$\langle\lambda'\|F_+F_-\|\lambda\rangle=\langle\lambda'\|F_-F_+\|\lambda\rangle$ [a]
±1	∓1	0	$\sqrt{2}(\delta_{m_b,0}+\delta_{m_b,\pm1})$
±1	0	∓1	$\delta_{m_4,\pm1/2}$
			$\times\sqrt{2}\,(\delta_{m_a,0}+\delta_{m_a,\mp1})\frac{1}{2}B'\frac{1}{4}(A'+B')$
0	±2	0	$2\,\delta_{m_b,\mp1}\frac{1}{16}(A'^2-B'^2)$
0	±1	∓1	$(\delta_{m_b,0}+\delta_{m_b,\mp1})\,\delta_{m_4,\pm1/2}\,\frac{1}{4}A'B'\sqrt{2}$

[a] This relation holds only when $\lambda'\neq\lambda$.

matrix elements of operator

$$W\equiv\langle N|VC_NV|N\rangle\ , \tag{A1}$$

where

$$C_N=\sum_{N'\neq N}\frac{|N\rangle\langle N'|}{E_N-E_{N'}}\quad\text{and}\quad V=\sum_n\mathcal{H}_F^{(n)}\ . \tag{A2}$$

Using relations (3) and (4), W can be written more explicitly as

$$W=\sigma_{zz}F_z^2+\sigma_{++}(F_-^2+F_+^2)+\sigma_{+-}F_-F_++\sigma_{-+}F_+F_-\ , \tag{A3}$$

with

$$\sigma_{q'q}\equiv\langle N|S_{q'}C_NS_q|N\rangle\quad(q,q'=z,+,-) \tag{A4}$$

and for orientation I [Fig. 1(a)] assuming the same A', B' values for all $\underline{A}'^{(n)}$, the nuclear spin operators F_q are given by

$$F_z=A'I_z^a+B'(I_z^b+I_z^{(4)})\ , \tag{A5}$$

$$F_\pm=\tfrac{1}{2}BI_\pm^a+\tfrac{1}{4}(A'+B')(I_\pm^b+I_\pm^{(4)})+\tfrac{1}{4}(A'-B')(I_\mp^b-I_\mp^{(4)})\ , \tag{A6}$$

where equivalent spins have been conveniently added, i.e., $\vec{I}^{(1)}+\vec{I}^{(2)}=\vec{I}^a$ and $\vec{I}^{(3)}+\vec{I}^{(5)}=\vec{I}^b$ [Fig. 1(a)].

In the

$$|I^a;m_a\rangle\,|I^b;m_b\rangle\,|m_4\rangle\equiv|\lambda\rangle$$

basis the diagonal elements required in the calculation are

$$W_{\lambda\lambda}=\sigma_{zz}[A'm_a+B'(m_b+m_4)]^2+\sigma_{++}\tfrac{1}{8}(A'^2-B'^2)[2I^b(I^b+1)-1-2m_b^2]+(\tfrac{1}{2}B')^2\{(\sigma_{+-}+\sigma_{-+})[I^a(I^a+1)-m_a^2]$$
$$-(\sigma_{+-}-\sigma_{-+})m_a\}+\tfrac{1}{8}(A'^2+B'^2)(\sigma_{+-}+\sigma_{-+})[I^b(I^b+1)-m_b^2+\tfrac{1}{2}]-\tfrac{1}{4}(A'B')(\sigma_{+-}-\sigma_{-+})(m_b+m_4)\ , \tag{A7}$$

whereas the nondiagonal elements $W_{\lambda\lambda'}$ can be obtained using Tables III and IV.

A straightforward 2×2 diagonalization handles the first-order degeneracy still present in the $|\lambda\rangle$ set ($V_{\lambda\lambda}-V_{\lambda'\lambda'}=0$, if $\Delta m_b=-\Delta m_4=\pm1$ and $\Delta m_a=0$) and yields the appropriate $|\nu\rangle$ functions.[12] $W_{\nu\nu}$ is the second-order correction to the energy levels and the intensity of transitions of the type $\nu'\neq\nu$ is given by

$$P(H_0)\left|\Delta\frac{W_{\nu'\nu}}{V_{\nu\nu}-V_{\nu'\nu'}}\right|^2\ ;$$

these transitions involve the reorientation of two nuclear spins (see Tables III and IV) and turned out to be far too small to be observable.

The $W_{\nu\nu}$'s are related to the second-order contribution to the shf displacement by

$$\delta H_2=-\frac{\Delta W_{\nu\nu}+\frac{1}{2}(\delta H_1)^2\,\Delta(d^2/dH_0^2)(E_N+V_{\nu\nu})}{\Delta(d/dH_0)(E_N+V_{\nu\nu})}\ , \tag{A8}$$

where δH_1 is given by Eq. (8) in the text. Clearly the determination of the sign of A' and B' from the asymmetries of the shf pattern, is possible only when $\Delta W_{\nu\nu}$ is large enough.

[1] K. N. Shrivastava and P. Venkateswarlu, Proc. Ind. Acad. Sci. A 63, 311 (1965).

[2] B. Bleaney and R. S. Rubins, Proc. Phys. Soc. (London) 77, 103 (1961); 78, 778 (1961).

[3] G. L. Bir, Fiz. Tverd. Tela 5, 2236 (1963) [Sov. Phys. Solid State, 5, 1628 (1964)].

[4] C. Marti, R. Romestain, and R. Visocekas, Phys. Status Solidi 28, 97 (1968).

[5] R. Böttcher, W. Windsch, and W. Lüdke, Phys. Status Solidi 20, 121 (1967).

[6] C. Gago-Bousquet, A. Serra-Valls, and M. García-Sucre, J. Magnetic Res. 6, 117 (1972).

[7] No direct proof has been found so far to identify the point defect along direction I [Fig. 1(a)] with a vacancy (Ref. 6). But this matter does not concern us here.

[8] A sample of this crystal was used in Ref. 6.

[9] G. Blanc, C. Gago-Bousquet, M. García-Sucre, and A. Serra-Valls, Acta Cient. Venezolana 20, 104 (1969); C. Gago-Bousquet, M. García-Sucre, and A. Serra-Valls, *ibid.* 21, 48 (1970).

[10] T. P. P. Hall, W. Hayes, R. W. Stevenson, and J. Wilkens, J. Chem. Phys. 38, 295 (1963).

[11] shf structures I and III were obtained taking $B'=0.5a'=13.7$ G and for structure II, $A'_4=24$ G and $B'_{\text{eff}}=16$ G (Ref. 6).

[12] E. P. Wigner, *Group Theory and its Application to the Quantum Mechanics of Atomic Spectra* (Academic, New York, 1959), Chap. 5.

[13] A rule similar to (9) holds also in cases when one of the $|N\rangle$ levels involved in the transition is nearly degenerate. In this case the factor f_1 may be somewhat affected. However, since the few transitions of this type

are of weak intensity or else their observation is hindered by allowed spectrum IV (Fig. 3) we shall not treat this effect here.

[14]T. G. Stoebe, J. Phys. Chem. Solids 28, 1375 (1967); A. Bianchini, M. Martinelli, S. Santucci, P. Bergé, and C. Laj, Phys. Letters A29, 522 (1969). Further, an unresolved nuclear interaction associated with X^- is suggested by the differences in Γ_{pp} found for structures I and II in Ref. 6.

[15]A way out of this difficulty could be found by means of an experiment in which the static and microwave magnetic fields are parallel. In this case all transitions would be of the forbidden type.

PHYSICAL REVIEW B VOLUME 6, NUMBER 7 1 OCTOBER 1972

Nuclear-Resonance Investigation of a Scandium-Hydrogen Solid Solution*

H. T. Weaver
Sandia Laboratories, Albuquerque, New Mexico 87115
(Received 9 May 1972)

Nuclear-magnetic-resonance measurements of spin-lattice relaxation time, Knight shift, and linewidths have been made for ^{1}H and ^{45}Sc contained in $ScH_{0.37}$. Rigid-lattice proton linewidths indicate that the hydrogen is randomly located among two interstitial sites in hcp scandium. Both the spin-lattice relaxation rate and Knight shift for ^{45}Sc decrease relative to the values for scandium metal in such a manner that the Korringa product remains constant. Diffusion parameters are determined from the proton data.

Nuclear-magnetic-resonance (NMR) methods have been used extensively to study transition-metal hydrides. Information relating to the electronic band structure[1,2] and hydrogen diffusion parameters[3-7] and at least some indication as to the atomic configuration[3,4] have been obtained. However, studies directed at intrinsic properties of hydrogen-metal systems as a function of hydrogen content are severely limited due to the large two-phase region present in most transition-metal hydrides.[8]

Scandium metal is unusual in that it can absorb relatively large amounts of hydrogen without undergoing a phase change.[8] Consequently, appreciable changes for the experimental properties relative to the elemental metal or hydride can be expected. The purpose of this paper is to report measurements of spin-lattice relaxation time, Knight shift, and linewidth measurements for ^{1}H and ^{45}Sc contained in $ScH_{0.37}$.

Spin-lattice relaxation times were measured by conventional phase-coherent techniques. Linewidths and Knight shifts were determined from spectra obtained using a Varian Model No. 4210 spectrometer. The shifts were measured at room temperature and the metal relaxation time was determined at 77 and 300 K. The resonance frequencies were 16 MHz for cw work and 25 and 10 MHz for ^{1}H and ^{45}Sc transient work, respectively.

The sample was prepared by exposing elemental scandium to hydrogen. Care was taken so that the hydrogen pressure never exceeded the equilibrium vapor pressure of the solid solution, so that no phase transition was likely. Subsequent x-ray patterns confirmed a hexagonal structure which was slightly expanded over scandium metal.

Both the Knight shift and spin-lattice relaxation rate for ^{45}Sc in $ScH_{0.37}$ decrease from the elemental metal values,[1,2] indicating a decrease in the density of states of the conduction electrons at the Fermi energy. Table I summarizes our results together with the metal and dihydride data. The Knight shift is found to be 0.14%, which is intermediate to the metal and dihydride values of 0.24 and 0.07%, respectively. Similarly, we estimate T_1T to be 4.9 sec K compared to 1.6 and 25 sec K for metal and dihydride, respectively.

Since the ^{45}Sc line is broadened by quadrupole interactions, considerable caution should be taken that the measured T_1 actually reflects the spin-lattice relaxation process. The low-power transmitter used in the present work was incapable of saturating the resonance even with the use of a combination of pulses. In view of this we employed a three-pulse sequence so that only $\frac{1}{2}$-$\frac{1}{2}$ transitions were excited. Under these conditions a system of spin $\frac{7}{2}$ yields $\frac{1}{28}$ T for the initial magnetization recovery rate.[9] Due to this procedure for finding T_1, its value should be regarded as approximate.

Nuclear-resonance parameters for ^{45}Sc in scandium metal undoubtedly reflect contributions from d as well as s states similar to other $3d$ metals.[9,10] Consequently, the monotonic decrease in K as hydrogen is added indicates a reduction in density of states for both these atomic symmetries. This conclusion can be made somewhat more quantitative by following the analysis of Schreiber.[1] In brief, he parametrizes the Korringa product as